

Magneto-Mechanical Model of Passive Magnetic Axial Bearings versus the Eccentricity Error, Part I: Physical Mathematical Model

Roberto Muscia

Department of Engineering and Architecture
University of Trieste, Trieste, Italy
muscia@units.it

Abstract — In this paper we illustrate a particular analytical numerical model of passive magnetic bearings with axial magnetization. The approach is based on the magnetic charges method. This method avoids the utilization of the finite element analysis. In relation to the system geometry, we find explicit formulations for computing magnetic fields by simple numerical integrations. A detailed magnetostatic model is developed and the nonlinearity of the magnetization vector \mathbf{M} of the ring magnets can be considered by a very simple modification of the equations illustrated. The equations can be immediately implemented in a mathematical software and only few minutes are sufficient to obtain the results.

Index Terms — Levitation, magnetic bearings, magnetostatic field, natural frequencies, stiffnesses.

I. INTRODUCTION

The magnetic levitation allows the suspension of one object above another without the two coming into contact. There are several studies and applications of this phenomenon [1], [2] and one of the best known is represented by passive magnetic bearings [3-6]. Generally these bearings can be of two types depending on the direction of polarization of the rings: axial or radial. In both cases, the forces that keep the rings separate are repulsive. Therefore, the rings of these bearings are arranged with the same poles facing each other. The value of these repulsive forces depends on the air gap between the facing surfaces. The air gap changes as a function of the applied forces. Consequently, it is possible to define a bearing stiffness which varies depending on the magnitude of the load applied and/or by the mutual position of the rings. Since the rotating rings of the magnetic bearings are always keyed to a shaft on which other elements are also fixed, an elastic system characterized by a certain stiffness and mass is defined. Therefore, we can evaluate the natural vibration frequencies of this mechanical system. These frequencies depend on the stiffness and mass suspended by the magnetic levitation. Since the stiffness changes with the

mutual position of each pair of facing rings, the stiffness and the natural frequency of the system vary versus the applied load. Thus, in general, with regard to each stationary working condition of the magnetic bearings, a natural frequency of the system is fixed. In this respect, we have developed a model based on magnetic charges to evaluate stiffnesses and natural frequencies of a magnetic levitation system with a passive axial magnetic bearing. We note that the same procedure can be easily extended to calculate the above mentioned stiffness and frequencies also for passive radial magnetic bearing.

II. CONFIGURATION OF THE SYSTEM

Figure 1 shows the case study. The polarized ring A is fixed. The moving ring of the bearing is denoted by B. The two rings have the facing surfaces polarized with the same pole. The polarized ring B can rotate around its own axis with a certain angular velocity ω and is positioned at a distance t from ring A. Therefore t is the air gap of the bearing. This air gap can also be considered as a translation degree of freedom of the system. The axes of the two rings are parallel but, in general not coaxial. An eccentricity e is defined: e represents a coaxiality error. The ring B supports a mass m whose value is equal to the sum of all the masses rigidly integral with the same ring B. The vertical force \mathbf{F} is the axial force applied to the bearing. The dashed segments a and b represent the two circumferences that pass through the section centers of gravity of the polarized rings. The sections of these rings have been considered to be identical for both rings A and B. The shape of the sections is rectangular. Figure 2 illustrates the magnetization vector \mathbf{M} of A and B. The \mathbf{M} direction is defined by different values of the angle α . Three cases have been considered: $\alpha = 90, 60, 30$ degrees. The discrete variability of the angle α has only been considered for illustrating a general procedure to obtain the equations of the field and the forces when the magnetization \mathbf{M} depends on the same α and possibly on the radius. For simplicity, such procedure is illustrated by fixing the module of \mathbf{M} to a constant value. Moreover, its direction does not change when the planes π_1 and π_2 ,

to which \mathbf{M} belongs, radially move towards or away from the respective axes of the magnets A and B (see Fig. 2). If \mathbf{M} depends on α and the radius r (the distance from the axes of the magnets), in all the integrals indicated in the following Section III, \mathbf{M} and the other quantities versus α and r must remain under the integral sign (in this case the magnetization model is not linear). Moreover, also the volume charge density $\rho_M(\mathbf{P})$ defined in the generic point P (end of the vector \mathbf{P}) of the permanent magnets has to be considered. In the case study (\mathbf{M} and α are constants), since the magnetization model is linear, the inclined magnetization can be decomposed in an axial and a circular component independent of α and r . The circular component defines a flux inside the magnet and does not generate any external magnetic field outside the same magnet. Therefore, the circular components of \mathbf{M} of the two polarized rings cannot interact since they produce no field and force outside the magnets. This consideration will be also illustrated by the numerical examples.

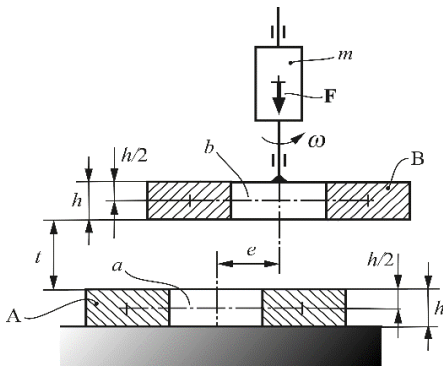


Fig. 1. Axially polarized rings with eccentricity e .

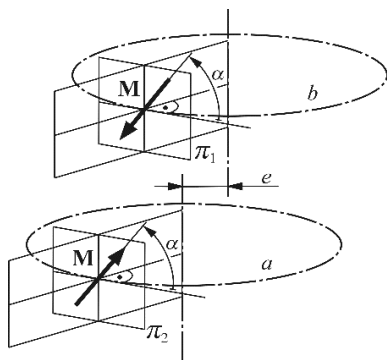


Fig. 2. Direction of the magnetization vectors \mathbf{M} in the two polarized rings.

III. EVALUATION OF THE MAGNETIC FIELD

The calculation of the levitation forces has been performed by using the magnetostatic model and the

magnetic charge method [7-9]. The surface charge density $\sigma_M(\mathbf{P})$ and the volume charge density $\rho_M(\mathbf{P})$:

$$\sigma_M(\mathbf{P}) \equiv \mathbf{M}(\mathbf{P}) \cdot \hat{\mathbf{n}}, \quad (1)$$

$$\rho_M(\mathbf{P}) \equiv -\nabla \cdot \mathbf{M}(\mathbf{P}), \quad (2)$$

were considered. This method can be considered a valid alternative to the finite element method that is often utilized [10], [11]. As a matter of fact, the time computation and the accuracy of the results can improve, even though an analytical formulation is necessary.

A. Surface charge density $\sigma_M(\mathbf{P})$ for the polarized rings A and B

In Fig. 3 an infinitesimal element of the magnet A is illustrated. The point P represents the center of the element. The element shows six infinitesimal faces denoted by dS_1, dS_2, \dots , and dS_6 . The correspondent normal versors are $\hat{\mathbf{n}}_1, \hat{\mathbf{n}}_2, \dots$, and $\hat{\mathbf{n}}_6$. The expressions of the versors can be suitably expressed versus the angle θ . The magnetization vector $\mathbf{M}(M_x, M_y, M_z)$ is applied to the point P of the infinitesimal magnet illustrated in Fig. 3. The moduli with the signs M_x, M_y , and M_z of the components of \mathbf{M} can be expressed versus the angles θ and α (see Fig. 4). By using Eq. (11), we obtain the six surface charge densities σ_{MAi} relative to the surfaces dS_i ($i=1, 2, \dots, 6$) of the infinitesimal magnet A:

$$\sigma_{MA1} = M \sin \alpha, \quad (3)$$

$$\sigma_{MA2} = -M \sin \alpha, \quad (4)$$

$$\sigma_{MA3} = -M \cos \alpha, \quad (5)$$

$$\sigma_{MA4} = M \cos \alpha. \quad (6)$$

For the surfaces dS_5 and dS_6 , σ_{MA5} and σ_{MA6} are equal to zero (\mathbf{M} is always perpendicular to the normal straight line of the surfaces dS_5 and dS_6). The surface charge densities σ_{MBi} of the polarized ring B are obtained by changing the sign of the σ_{MAi} .

B. Volume charge density $\rho_M(\mathbf{P})$ for the polarized rings A and B

By observing Figs. 3 and 4 we obtain:

$$M_x = -M \cos \alpha \frac{p_y}{\sqrt{p_x^2 + p_y^2}}, \quad (7)$$

and

$$M_y = M \cos \alpha \frac{p_x}{\sqrt{p_x^2 + p_y^2}}, \quad (8)$$

where p_x, p_y , and p_z are the components of the vector \mathbf{P} that identifies the point P. By using Eq. (2) and by deriving

Eqs. (7) and (8) with respect to p_x , and p_y , respectively, we obtain:

$$\frac{\partial M_x}{\partial p_x} = M \cos \alpha \frac{p_x p_y}{(p_x^2 + p_y^2)^{3/2}}, \quad (9)$$

and

$$\frac{\partial M_y}{\partial p_y} = -M \cos \alpha \frac{p_x p_y}{(p_x^2 + p_y^2)^{3/2}}. \quad (10)$$

The partial derivative $\partial M_z / \partial p_z$ is equal to zero. By substituting Eqs. (9), (10), and $\partial M_z / \partial p_z = 0$ in Eq. (2), we note that volume charge density $\rho_{MA}(\mathbf{P})$ is always equal to zero. For the magnet B we obtain the same result, i.e., $\rho_{MB}(\mathbf{P}) = 0$, whatever the value of α is.

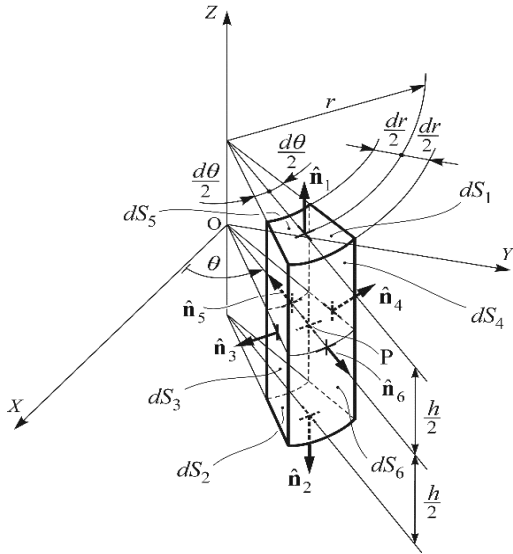


Fig. 3. Infinitesimal element of the polarized ring A with versors outgoing from the surfaces.

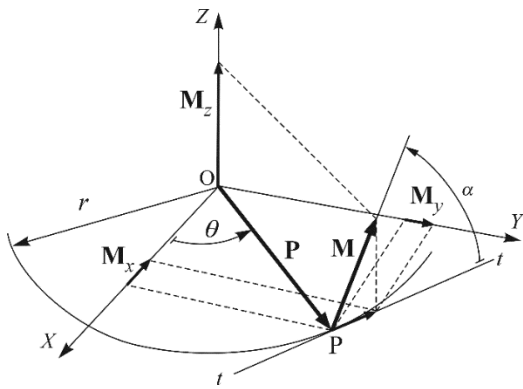


Fig. 4. Magnetization vectors components \mathbf{M}_x , \mathbf{M}_y , and \mathbf{M}_z , in the generic point P of the magnet A (see Fig. 3). $t-t$ is the tangent to the circumference of radius r in P (\mathbf{P} is always perpendicular to $t-t$).

C. Surfaces dS_1, dS_2, \dots , and dS_4

In order to evaluate the magnetic induction generated by the magnet A and the forces/moments applied to the magnet B, since σ_{MA5} , σ_{MB5} , σ_{MA6} , and σ_{MB6} are equal to zero, we evaluate the only expressions of the surfaces dS_1, dS_2, \dots , and dS_4 . By observing Fig. 5, we can define the expressions of the infinitesimal surfaces dS_i with $i=1, 2, \dots, 4$ versus $d\theta$, dr and h . Denoting by $\mathbf{P}_i(p_{xi}, p_{yi}, p_{zi})$ the vectors that identify the centers P_i of the above-mentioned surfaces dS_i , we obtain the expression of the components p_{xi} , p_{yi} , and p_{zi} in function of θ , r and h .

D. Evaluation of the magnetic induction $\mathbf{B}(\mathbf{P}')$

In order to evaluate forces and moments applied to the magnet B, four contributions $\mathbf{B}_1(\mathbf{P}')$, $\mathbf{B}_2(\mathbf{P}')$, \dots , $\mathbf{B}_4(\mathbf{P}')$ of the magnetic induction have to be considered. \mathbf{P}' is the vector that identifies the point where the magnetic induction will be computed is given by [4]:

$$\mathbf{B}_i(\mathbf{P}') = \frac{\mu_0}{4\pi} \int_{S_i} \frac{\sigma_{MA_i}(\mathbf{P})(\mathbf{P}' - \mathbf{P})}{|\mathbf{P}' - \mathbf{P}|^3} dS_i, \quad (11)$$

with $i=1, 2, \dots, 4$. μ_0 is the free space permeability. The volume contribution to $\mathbf{B}_i(\mathbf{P}')$ is always equal to zero because $\rho_{AM}(\mathbf{P}) = 0$. By substituting Eqs. (3)-(6) and the expressions of p_{xi} , p_{yi} , and p_{zi} versus θ , r and h in Eq. (11), we achieve the components $B_{xi}(\mathbf{P}')$, $B_{yi}(\mathbf{P}')$, and $B_{zi}(\mathbf{P}')$ of $\mathbf{B}_i(\mathbf{P}')$. For example, the components $B_{xi}(\mathbf{P}')$ is the following:

$$B_{xi}(\mathbf{P}') = \frac{\mu_0 M \sin \alpha}{4\pi} \int_0^{2\pi} \int_{r_i}^{r_e} \frac{(p'_x - r \cos \theta) r}{\left[(p'_x - r \cos \theta)^2 + (p'_y - r \sin \theta)^2 + (p'_z - h/2)^2 \right]^{3/2}} d\theta dr. \quad (12)$$

The other components have a similar formulation. The components $B_x(\mathbf{P}')$, $B_y(\mathbf{P}')$ and $B_z(\mathbf{P}')$ of the resultant magnetic induction $\mathbf{B}(\mathbf{P}')$ in the generic point \mathbf{P}' of the B magnet surfaces are obtained by adding the correspondent components $B_{xi}(\mathbf{P}')$, $B_{yi}(\mathbf{P}')$, and $B_{zi}(\mathbf{P}')$ with $i=1, 2, \dots, 4$. Since the sign of $B_{xi}(\mathbf{P}')$, $B_{yi}(\mathbf{P}')$, and $B_{zi}(\mathbf{P}')$ is opposite to the sign of $B_{xi+1}(\mathbf{P}')$, $B_{yi+1}(\mathbf{P}')$, and $B_{zi+1}(\mathbf{P}')$, respectively, when i is equal to 3 and 4 and the corresponding moduli are equal to each other, we have:

$$B_x(\mathbf{P}') = B_{x1}(\mathbf{P}') + B_{x2}(\mathbf{P}'), \quad (13) \quad \text{and analogous expressions of } B_y(\mathbf{P}') \text{ and } B_z(\mathbf{P}').$$

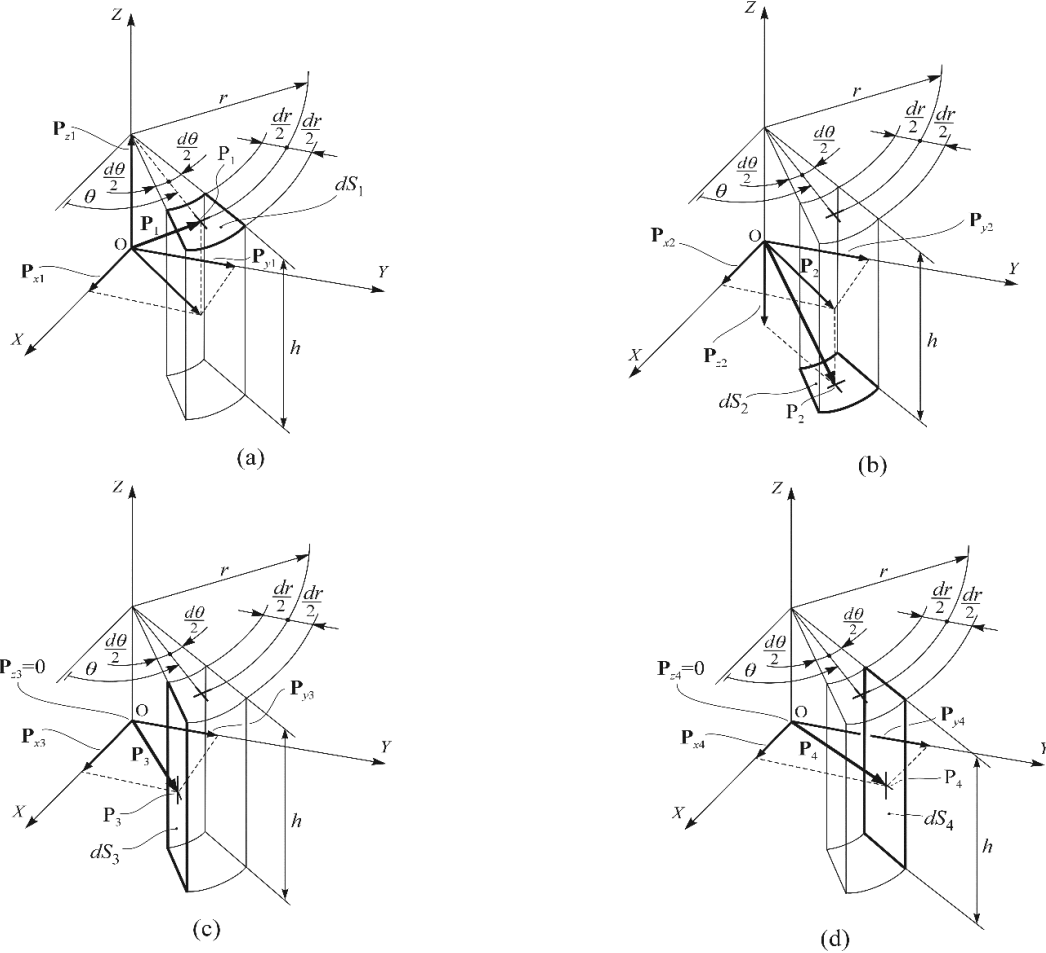


Fig. 5. Evaluation of: (a) dS_1 , (b) dS_2 , (c) dS_3 , and (d) dS_4 with the relative P_1 , P_2 , P_3 , and P_4 centres (see also Fig. 3) in the magnet A.

IV. EVALUATION OF FORCES AND MOMENTS APPLIED TO THE POLARIZED RING B

With reference to Fig. 6, the infinitesimal resultant force $d\mathbf{F}$ applied from the magnet A to a generic infinitesimal element of the magnet B is obtained by adding four force $d\mathbf{F}_i$ ($i=1, 2, \dots, 4$):

$$d\mathbf{F} = d\mathbf{F}_1 + d\mathbf{F}_2 + d\mathbf{F}_3 + d\mathbf{F}_4. \quad (14)$$

Each of them is applied to the correspondent surfaces dS_i that define the infinitesimal element of the polarized ring B (see Fig. 6). We observe that these surfaces have the same expressions of the correspondent surfaces defined for the magnet A. Since the surfaces charges densities σ_{MB5} and σ_{MB6} are equal to zero, the surfaces dS_5 and dS_6 relative to the ring B do not give any contribution to $d\mathbf{F}$. By denoting $\mathbf{P}'_i(p'_{xi}, p'_{yi}, p'_{zi})$ the vectors that identify the centers P'_i of the above-mentioned surfaces dS_i ($i=1, 2, \dots, 4$), we can define the expressions of p'_{xi} ,

p'_{yi} , and p'_{zi} versus p_{xi} , p_{yi} , p_{zi} , e , and t (see Fig. 6). The forces $d\mathbf{F}_i$ are applied to the points P'_i . The evaluation of $d\mathbf{F}_i$ is performed by the following relation:

$$d\mathbf{F}_i = \sigma_{Bi}(\mathbf{P}'_i)\mathbf{B}(\mathbf{P}'_i) dS_i, \quad (15)$$

where $i=1, 2, \dots, 4$. By using Eq. (13) and the analogous expressions of $B_y(\mathbf{P}')$ and $B_z(\mathbf{P}')$, integrating Eq. (15), we compute the moduli with the signs F_{xi} , F_{yi} , and F_{zi} of the \mathbf{F}_i components. For example, the components F_{x1} and F_{x3} are the following:

$$F_{x1} = -M \sin \alpha \int_0^{r_i} \int_0^{2\pi} B_x(\mathbf{P}'_1) r d\theta dr, \quad (16)$$

$$F_{x3} = M \sin \alpha \int_r^r \int_x^x B_x(\mathbf{P}'_3) h dr. \quad (17)$$

The other components have an analogous formulation. Therefore, by adding the four forces \mathbf{F}_i (F_{xi} , F_{yi} , F_{zi}) we obtain the resultant force applied to the ring B.

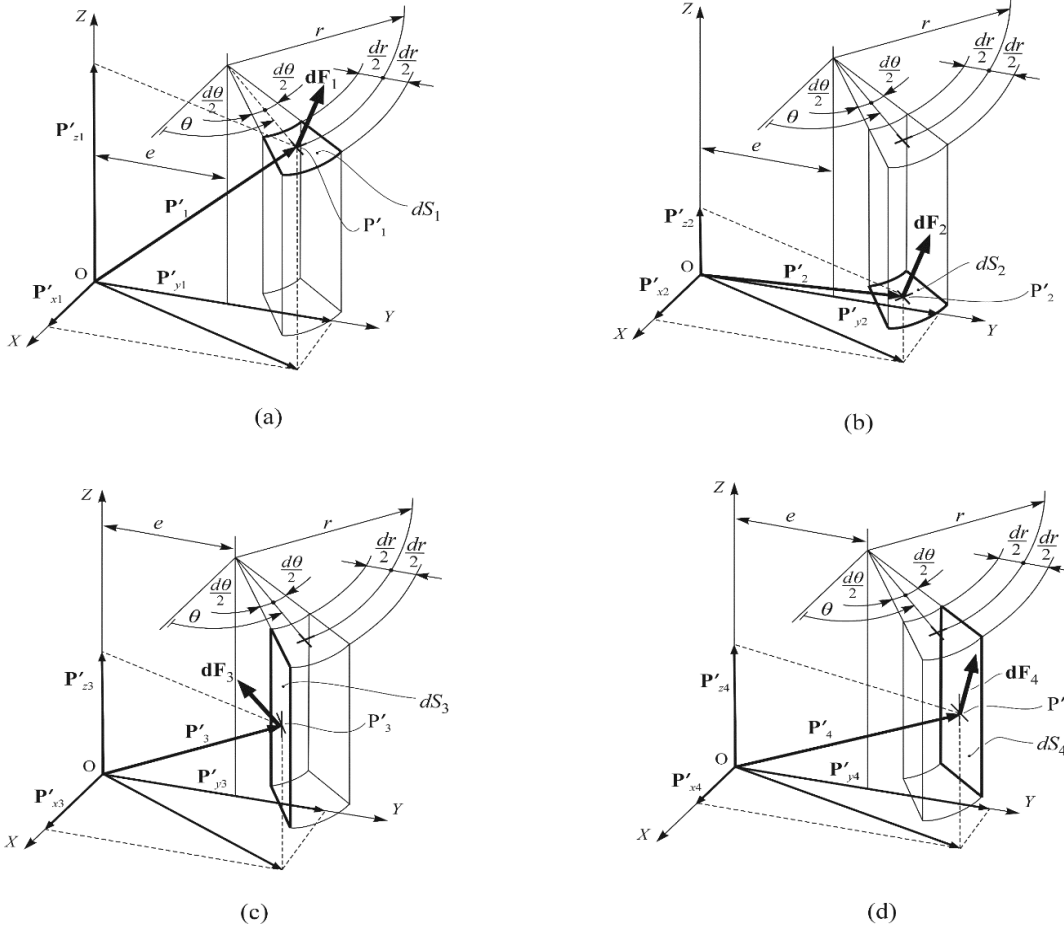


Fig. 6. Infinitesimal forces: (a) $d\mathbf{F}_1$, (b) $d\mathbf{F}_2$, (c) $d\mathbf{F}_3$, and (d) $d\mathbf{F}_4$ applied to the corresponding centres P_1 , P_2 , P_3 , and P_4 of the surfaces dS_1 , dS_2 , dS_3 , and dS_4 of the infinitesimal element of the magnet B.

V. EVALUATION OF THE TORQUE APPLIED TO THE POLARIZED RING B

In order to check the correctness of the physical mathematical model, it is suitable to verify the law of energy conservation. This check can be performed by computing the moment component τ_z along the axis Z applied from the ring A to the ring B. τ_z must always be equal to zero, whatever the values of α and e are. If this condition is not met, the law of energy conservation is not verified and the model is wrong (the ring B spontaneously rotates). The computation of τ_z is performed by integrating the following relation:

$$d\tau_z = d\tau_{z1} + d\tau_{z2} + d\tau_{z3} + d\tau_{z4}, \quad (18)$$

where

$$d\tau_{zi} = d\mathbf{F}_i \times \mathbf{P}'_i, \quad (19)$$

and $i=1, 2, \dots, 4$. $d\tau_{zi}$ represents the moment around the axis Z generated from the force $d\mathbf{F}_i$ applied to the

corresponding surface dS_i of the infinitesimal element of the ring B. Therefore, by Eqs. (18) and (19) we obtain the following modulus with sign of τ_z :

$$\begin{aligned} \tau_z = M \sin \alpha \int_0^{2\pi} \int_{r_i}^{r_e} r [B_x(r \cos \theta, r \sin \theta + e, \frac{h}{2} + h + t)(r + e) \sin \theta - \\ B_y(r \cos \theta, r \sin \theta + e, \frac{h}{2} + h + t) r \cos \theta] - \\ r [B_x(r \cos \theta, r \sin \theta + e, \frac{h}{2} + t)(r + e) \sin \theta - \\ B_y(r \cos \theta, r \sin \theta + e, \frac{h}{2} + t) r \cos \theta] d\theta dr. \end{aligned} \quad (20)$$

In relation to the law of energy conservation the value of τ_z computed by Eq. (20) must be equal to zero, whatever the angle α of the magnetization \mathbf{M} is (see Fig. 2). Eq. (20) has been numerically evaluated and in Part II we briefly discuss this aspect. The values of τ_z versus α and e obtained are very small and confirm the

previous statement.

VI. AXIAL/RADIAL STIFFNESSES AND NATURAL FREQUENCIES

A. Stiffnesses

In general, the computation of the stiffness K is based on the following relation:

$$K = \frac{\partial F(p)}{\partial p}, \quad (21)$$

where $F(p)$ is the force versus the parameter p that defines the degree of freedom (DOF) along which the stiffness is computed. In the present study we evaluate the axial stiffness K_t along the axis Z versus the air gap t :

$$K_t = \frac{\partial F_z(t)}{\partial t}, \quad (22)$$

and the radial stiffness K_e along the axis Y where the eccentricity e is defined:

$$K_e = \frac{\partial F_y(e)}{\partial e}. \quad (23)$$

The evaluation of K_e can be interesting also when we study an axial magnetic bearing. As a matter of fact, K_e has to be considered together with the other radial stiffnesses of the two radial bearings keyed on the shaft. The dynamic behaviour of the system also depends on K_e .

B. Natural frequencies

The natural frequencies of a system depend on its mass and stiffness. From the modelization point of view, the number of these frequencies is equal to the number of degrees of freedom of the model. In relation to the device schematized in Fig. 1, we can consider various models. The choice of the model is strictly connected to the dynamic behaviour of the real system that we want study. If a rigid body schematization of the real system is acceptable and the radial bearings of the vertical shaft have a very high radial stiffness, we can modelize the structure by one degree of freedom (DOF) model (the DOF along the axis Z). If the flexural stiffness of the shaft is not high and there are radial excitation forces, it is necessary to introduce new DOFs. Moreover, also if the radial stiffness of the radial bearing is not high, other radial DOFs associated with these bearing have to be considered. We observe that the system can become very complex. The vibrational behavior will depend on nonlinear magnetic stiffnesses and also small chaotic precessional motions can rise. In a demanding practical application, this kind of motions can be due to the alignment errors of the shaft (concentricity, circularity, perpendicularity, plumb, straightness, see Fig. 7 [12]). In the present study we can limit ourselves to two simple cases. The first one considers a model with a DOF only along the axis Z . In the second case the model has a DOF

only along the axis Y . The two models are illustrated in Figs. 8 (a) and 8 (b), respectively. The model of Fig. 8 (a) can be used to study the dynamical behaviour of a device where all the stiffnesses are much higher than the stiffness K_t defined by Eq. (22). In Fig. 8 (a) m_{tot} represents the total suspended mass. Conversely, Fig. 8 (b) shows a model to study a system with a shaft that can only horizontally translate. By this schematization we again assume that the stiffness of all parts of the device are very high with respect to the radial stiffness K_e furnished by Eq. (23). In this case the translation DOF could be due to the radial clearances of the radial bearings. These clearances would allow a small horizontal translation of the rigid shaft. Therefore, the shaft horizontally translates during its rotation. Small rotations around the centres of the bearing could also occur. Nevertheless, if the flexural stiffness of the shaft is high, in general the influence of the corresponding rotational DOFs on the vibration behavior is negligible. With reference to this hypothesis and overall for simplicity, we can consider the simplified model illustrated in Fig. 8 (b). The system would normally be studied by using complex modelizations based on rotor dynamics (see, for example, [13]). The four masses indicated in Fig. 8 (b) represent the point masses to modelize, for example, the rotating mass of a hydrounit for electric generation (see Fig. 9 [12]). If we assume to substitute the oleodynamic thrust bearing (see particular C in Fig. 9) with a passive magnetic axial bearing (see Fig. 1), we can suitably fix the values of m_1, m_2, \dots , and m_4 versus the masses of the various rotating parts of the hydrounit [mass of the thrust bearing, shafts, rotor, turbine (not illustrated), etc.]. Therefore, the mass of the polarized ring B indicated in Fig. 1 contributes to defining the mass m_2 shown in Fig. 8 (b). With reference to the two models illustrated in Fig. 8 we evaluate the corresponding natural angular frequencies ω_{em_h} , $\omega_{em_{tot}}$, ω_{tm_h} , and $\omega_{tm_{tot}}$ of the system by the following relations:

$$\omega_{em_h} = \sqrt{\frac{K_e(e)}{m_1 + m_2 + m_3 + m_4}}, \quad (24)$$

$$\omega_{em_{tot}} = \sqrt{\frac{K_e(e)}{m_{tot}}}, \quad (25)$$

$$\omega_{tm_h} = \sqrt{\frac{K_t(t)}{m_1 + m_2 + m_3 + m_4}}, \quad (26)$$

$$\omega_{tm_{tot}} = \sqrt{\frac{K_t(t)}{m_{tot}}}. \quad (27)$$

As soon as m_{tot}, m_1, m_2, \dots , and m_4 have been fixed and the stiffnesses K_t and K_e are known [see Eqs. (22) and (23)], we can compute the natural angular frequencies

versus the air gap t and the eccentricity e [when we evaluate $K(t)$ we fix a certain value of e and vice versa].

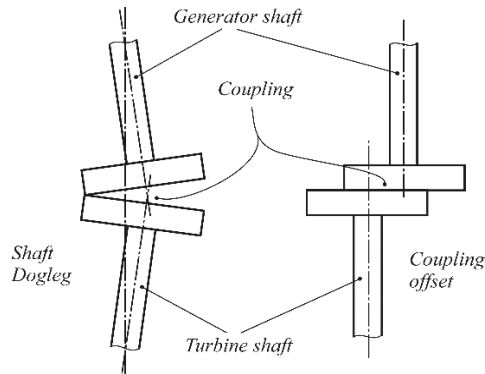


Fig. 7. Alignment errors of a turbine and generator shafts of a hydrounit [12].

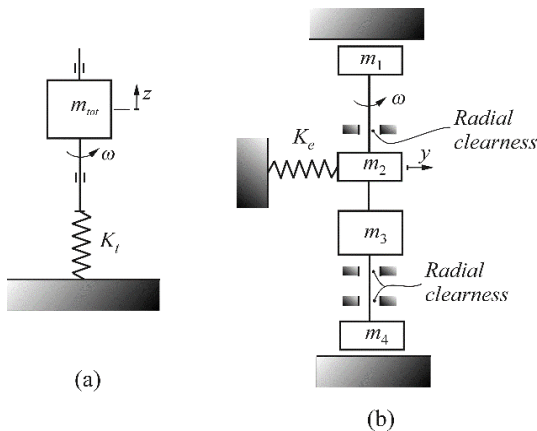


Fig. 8. Simplified physical model of the system with one (a) vertical and (b) horizontal DOF.

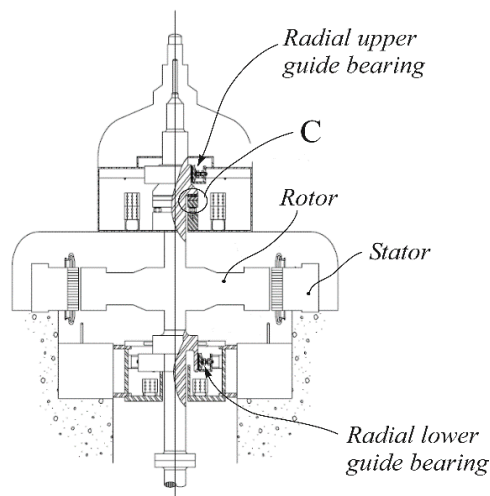


Fig. 9. A typical vertical disposition rotor/stator with thrust bearing C of a hydrounit for electric generation [12].

VII. CONCLUSION

A detailed formulation for evaluating forces, moments, stiffnesses and natural frequencies of a thrust magnetic bearing has been presented. Equations for checking the correctness of the analysis based on the magnetic charges method was considered. A mechanical model referred to a vertical disposition of a hydrounit for electric generation for performing the numerical calculations illustrated in Part II has been developed.

REFERENCES

- [1] H. Li, S. Wang, H. He, Y. Huangfu, and J. Zhu, "Electromagnetic – thermal – deformed – fluid – coupled simulation for levitation melting of titanium," *IEEE Transactions on Magnetics*, vol. 52, no. 3, 7402104, 2016.
- [2] Z. J. Sun, B. Ye, Y. Qiu, X. G. Cheng, H. H. Zhang, and S. Liu, "Preliminary study of a legged capsule robot actuated wirelessly by magnetic torque," *IEEE Transactions on Magnetics*, vol. 50, no. 8, 5100706, 2014.
- [3] J. P. Yonnet, "Passive magnetic bearings and couplings", *IEEE Transactions on Magnetics*, vol. 17, pp. 1169-1173, 1981.
- [4] E. P. Furlani, "A formula for the levitation force between magnetic disks," *IEEE Transactions on Magnetics*, vol. 29, pp. 4165-4169, 1993.
- [5] E. Tripodi, A. Musolino, A. R. Rizzo, and D. Casini, "Stability analysis of a new passive PMS bearing," *Proceedings of ISMB14*, Linz, Austria, August 11-14, 2014.
- [6] E. Rodriguez, J. Santiago, J. Pérez-Loya, F. S. Costa, G. Guilherme, J. G. Oliveira, and R. M. Stephan, "Analysis of passive magnetic bearings for kinetic energy storage systems," *Proceedings of ISMB14*, Linz, Austria, August 11-14, 2014.
- [7] W. F. Brown, Jr., "Electric and magnetic forces: A direct calculation I," *Am. J. Phys.*, vol. 19, pp. 290-304, 1951.
- [8] W. F. Brown, Jr., "Electric and magnetic forces: A direct calculation II," *Am. J. Phys.*, 19, pp. 333-350, 1951.
- [9] E. Furlani, *Permanent Magnets and Electromechanical Devices*. Academic Press, New York, 2001.
- [10] S. Wu, S. Zuo, X. Wu, F. Lin, and J. Shen, "Magnet modification to reduce pulsating torque for axial flux permanent magnet synchronous machines," *ACES Journal*, vol. 31, no. 3, pp. 294-303, March 2016.
- [11] Y. Chen and K. Zhang, "Electromagnetic force calculation of conductor plate double Halbach permanent magnet electrodynamic suspension," *ACES Journal*, vol. 29, no. 11, pp. 916-922, November 2014.
- [12] D. Temple, W. Duncan, and R. Cline, "Alignment of vertical shaft hydrounits," *Hydroelectric Re-*

search and Technical Service Group, Facilities Instructions, Standards and Technique, vol. 2-1, United States Department of the Interior Bureau of Reclamation, Denver, Colorado, 2000.

- [13] S. Y. Yoon, Z. Lin, and P. E. Allaire, *Chapter 2 – Introduction to Rotor Dynamics, in Control of Surge in Centrifugal Compressors by Active Magnetic Bearings*. Springer, London, pp. 17-55, 2013.

Supplementary materials

All the details of the analytical formulations can be requested to the author at muscia@units.it.



Roberto Muscia Professor at the University of Trieste, Trieste, Italy. He received his Master's degree in Mechanical Engineering from the University of Trieste in 1981. From 1983 to 1998 he was Researcher with the same university. From 1998 he is Associate Professor. At the present time his research interests focus on the study of mechanical problems in magnetic devices to improve their design.